MedChemComm

Accepted Manuscript

This is an *Accepted Manuscript*, which has been through the Royal Society of Chemistry peer review process and has been accepted for publication.

Accepted Manuscripts are published online shortly after acceptance, before technical editing, formatting and proof reading. Using this free service, authors can make their results available to the community, in citable form, before we publish the edited article. We will replace this *Accepted Manuscript* with the edited and formatted *Advance Article* as soon as it is available.

You can find more information about *Accepted Manuscripts* in the Information for Authors.

Please note that technical editing may introduce minor changes to the text and/or graphics, which may alter content. The journal's standard Terms & Conditions and the Ethical guidelines still apply. In no event shall the Royal Society of Chemistry be held responsible for any errors or omissions in this *Accepted Manuscript* or any consequences arising from the use of any information it contains.

ROYAL SOCIETY OF CHEMISTRY

www.rsc.org/medchemcomm

Tricyclic phenothiazine and phenoselenazine derivatives as potential multi-targeting agents to treat Alzheimer's disease

Gary Tin, [a] Tarek Mohamed, [a, b], Nyasha Gondora, [a] Michael A. Beazely, [a] and Praveen P. N. Rao, [a,*]

Graphical Abstract

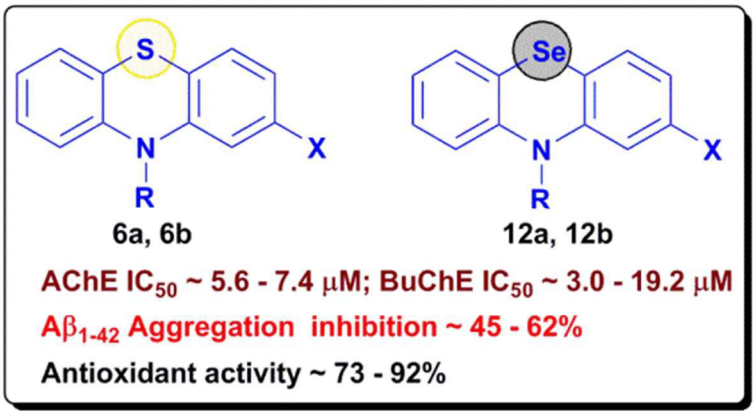

*Corresponding author:

Tel: +1 519 888 4567 ext: 21317; e-mail: praopera@uwaterloo.ca

[a]School of Pharmacy, Health Sciences Campus, University of Waterloo, 200 University Avenue West, Waterloo, Ontario, Canada N2L 3G1

[b]Department of Chemistry, University of Waterloo, 200 University Avenue West, Waterloo, Ontario, Canada N2L 3G1

Tricyclic phenothiazine and phenoselenazines as potential multi-targeting agents to treat Alzheimer's disease

Gary Tin, [a] Tarek Mohamed, [a, b] Nyasha Gondora, [a] Michael A. Beazely, [a] and Praveen P. N. Rao, [a,*]

[a] *School of Pharmacy, Health Sciences Campus, University of Waterloo, 200 University Avenue West, Waterloo, Ontario, Canada N2L 3G1*

[b] *Department of Chemistry, University of Waterloo, 200 University Avenue West, Waterloo, Ontario, Canada N2L 3G1*

A group of tricyclic phenothiazine (**6a**, **6b**, **7a–l**) and phenoselenazines (**12a**, **12b**, **13a–l**) were designed, synthesized and evaluated as multi-targeting ligands aimed at the cholinergic, amyloid and oxidative stress pathways of Alzheimer's disease. The phenothiazine derivative **7j** (2-chloro-10*H*-phenothiazin-10-yl-(4-methoxyphenyl)methanone), was identified as the best dual, nonselective cholinesterase inhibitor (AChE IC_{50} = 5.9 ± 0.6 μM; BuChE IC_{50} = 5.3 ± 0.5 μM), whereas in the corresponding phenoselenazine series, **13j** (2-chloro-10*H*-phenoselenazin-10-yl-(4-methoxyphenyl)methanone) exhibited good nonselective cholinesterase inhibition (AChE IC_{50} = 5.8 ± 0.4 μM; BuChE IC_{50} = 4.9 ± 0.5 μM). Interestingly, *N*-10 unsubstituted phenothiazine **6a** (AChE IC_{50} = 7.3 ± 0.6 μM; BuChE IC_{50} = 5.8 ± 0.5 μM; $A\beta_{1\text{-}42}$ aggregation inhibition = 62%; DPPH scavenging = 92%), and the corresponding phenoselenazine bioisotere **12a** (AChE IC_{50} = 5.6 ± 0.4 μM; BuChE IC_{50} = 3.0 ± 0.5 μM; $A\beta_{1\text{-}42}$ aggregation inhibition = 45.6%; DPPH scavenging = 84.4%), were able to exhibit multi-targeting ability by demonstrating cholinesterase inhibition, beta-amyloid aggregation and antioxidant properties. These results show that fused tricyclic ring systems based on either a phenothiazine or phenoselenazine

templates can be useful to develop hybrid small molecules to target multiple pathological routes associated with Alzheimer's disease.

---

1. Introduction

Alzheimer's disease (AD) is a complex neurodegenerative disorder that is the leading cause of dementia around the world.[1–3] Recent years have seen a dramatic rise in its prevalence due to an increase in the aging population, increasing life span and limited pharmacotherapy options. The cholinesterase inhibitors such as donepezil, galantamine and rivastigmine which prevent the degradation of the neurotransmitter acetylcholine (ACh), (by inhibiting the enzymes acetyl and butyrylcholinesterase AChE and BuChE respectively), yet provide only symptomatic relief and are ineffective as long term therapies for AD.[4–6] The enzyme AChE is primarily responsible for the degradation of the neurotransmitter ACh. However, as AD progresses, BuChE is known to take over this function due to depletion of AChE. These observations highlight the benefits of developing dual AChE and BuChE inhibitors. AD pathophysiology suggests the involvement of few major pathways such as cholinergic dysfunction, amyloid aggregation, tau hyperphosphorylation and oxidative stress, that can lead to neurodegeneration, loss of memory and cognition.[7–14] The involvement of multiple factors in the pathophysiology of AD supports the development of hybrid small molecules as multi-targeting agents to treat AD.[15–17]

Tacrine (Fig. 1, **1**), the first cholinesterase inhibitor, is an example of a fused tricyclic ring. Its chemical structure has been modified to design tacrine derivatives that exhibit multi-targeting ability as shown in Fig. 1 (**2** and **3**).[18, 19] In this regard, we investigated the use of phenothiazine (PTZ), and its bioisostere, phenoselenazine (PSZ, Fig. 1, **4** and **5**) derivatives, as multi-targeting ligands to treat AD, since they also possess a fused tricyclic ring system similar to tacrine. PTZs

represent an important class of bioactive molecules. For example, both chlorpromazine and fluphenazine are used in clinical therapy as antipsychotics.[20, 21] In addition, PTZ derivatives are also known to exhibit cholinesterase inhibition and antioxidant properties.[22-24]

The trace element selenium (Se) is an essential micronutrient in the diet and is known to be present in selenoproteins, such as glutathione peroxidase (GPx), which is part of body's antioxidant defense.[25] Interestingly a recent study in AD patients shows lower levels of selenium in the plasma, erythrocytes, and nails compared to the control group, suggesting that Se deficiency is associated with AD.[26] In this regard, some novel organoselenium compounds have been developed as multi-targeting compounds to treat AD, which further supports the incorporation of selenium to design novel anti-AD molecules.[27, 28] Based on this evidence, we considered the organoselenium based PSZ derivatives in our study as a bioisostere of sulfur containing PTZs.

Fused tricyclic ring systems based on either a PTZ or a PSZ have the potential to serve as suitable ring templates to design novel small molecule multi-targeting agents against AD pathophysiology. In our study, we synthesized a library of PTZ and PSZ derivatives which were evaluated for their potential to (i) inhibit AChE and BuChE enzymes; (ii) prevent amyloid aggregation and (iii) possess antioxidant properties. The structure activity relationship (SAR) data acquired demonstrates that PTZ and PSZ derivatives have the ability to inhibit cholinesterases, exhibit anti-amyloid aggregation and antioxidant properties as well as represent a novel class of fused tricyclic ring systems as multi-targeting ligands to treat AD.

2. Results and discussion

2.1 Chemistry

PTZ derivatives **7a**–**l** were synthesized starting from either unsubstituted 10*H*-phenothiazine (**6a**) or 2-chloro-10*H*-phenothiazine (**6b**), which were coupled to various acid chlorides (RCOCl, where R = phenyl, benzyl, phenethyl, 3- or 4-methoxyphenyl or 3,4-dimethoxyphenyl) under reflux at 110 °C in toluene as shown in Scheme 1.[29] These conditions afforded **7a**–**l** in good yields ranging from 70–95%. The synthesis of PSZ derivatives was accomplished in a stepwise fashion. Initially, the starting precursor diphenylamine (**11a** or **11b**) was synthesized by coupling cyclohex-2-enone (**8**) with iodine in presence of dimethylaminopyridine (DMAP) and potassium carbonate (K_2CO_3) to afford α-iodinated 2-cyclohex-2-enone (**9**) in 70% yield (Scheme 2).[30] In the next step, **9** was coupled with substituted anilines (**10**) in a metal-free approach by refluxing overnight in presence of trace amounts of *para*-toluenesulfonic acid (*p*-TSOH) to afford **11a** and **11b** in 40-50% yields.[31] The ring closing of **11a** or **11b** to obtain the PSZ tricyclic ring was achieved by heating them at 150 °C in a pressure vial, in presence of selenium, selenium dioxide (SeO_2) and iodine, using sulfolane as solvent.[32] It should be noted that the presence of SeO_2 helps in regenerating selenium in situ and improves the PSZ yield. The final yield of PSZ derivatives **12a** and **12b,** were 20–25% which was much better than our previous attempts to cyclize diphenylamine (**11a** or **11b**) in presence of selenium monochloride (Se_2Cl_2), under reflux, which provided poor yields (5–10%) and difficulty in purification.[33] In the final step, the PSZ derivatives **12a** and **12b,** were subjected to nucleophilic addition/elimination reaction with acid chlorides (RCOCl, where R = phenyl, benzyl, phenethyl, 3- or 4-methoxyphenyl or 3,4-dimethoxyphenyl), to afford PSZ derivatives **13a**–**l** in moderate to good yields (20–80%, Scheme 1).

2.2 Cholinesterase inhibition studies

The cholinesterase inhibition activity profile of PTZ (**6a**, **6b**, **7a–l**) and PSZ derivatives (**12a**, **12b**, **13a–l**) toward both human AChE and BuChE enzymes, were evaluated using the Ellman assay as per our previously reported protocol (Table 1).[34] The unsubstituted PTZ derivative **6a**, exhibited an IC_{50} value of 7.4 ± 0.6 μM toward human AChE and was less potent compared to reference agents tacrine (AChE IC_{50} = 0.16 ± 0.01 μM), donepezil (AChE IC_{50} = 0.04 ± 0.002 μM) and galantamine (AChE IC_{50} = 2.6 ± 0.6 μM, Table 1). Addition of an *N*-10 benzoyl substituent in compound **7a** (R = phenyl), retained AChE inhibition (IC_{50} = 8.0 ± 0.7 μM) and the compound was less potent compared to **6a**. The effect of *N*-10 aromatic acyl groups, with one and two carbon spacers, was explored. These modifications provided AChE inhibition for compounds **7b** (R = benzyl; AChE IC_{50} = 7.4 ± 0.8 μM) and **7c** (R = phenethyl; AChE IC_{50} = 7.1 ± 0.8 μM), although they were less potent compared to reference agents. Our previous work, has shown that the presence of a 3,4-dimethoxyphenyl substituent provided good cholinesterase inhibition.[34] Accordingly, the effect of methoxyphenyl substituents was explored by evaluating compounds **7d–f** (Table 1). Interestingly, these compounds exhibited AChE inhibition ranging from 5.8 to 6.3 μM (IC_{50}s), and were more potent compared to compounds **6a** and **7a–c**. The 3,4-dimethoxyphenyl compound (**7f**) was identified as the most potent AChE inhibitor (IC_{50} = 5.8 ± 0.4 μM). Furthermore, the addition of C-2 chlorine to the PTZ scaffold was investigated. It appears that C-2 chlorine substituent was not a major factor in AChE inhibition and C-2 chloro-PTZ derivatives **6b** and **7g–l**, exhibited IC_{50} values in the range of 4.6 to ~10.0 μM (Table 1). Similar to compounds from the non-chlorinated PTZ series (**6a** and **7a-c**), the presence of methoxyphenyl substituents enhanced AChE inhibition (**7j–l**) with compound **7k** (3-methoxyphenyl) identified as the most potent compound (AChE IC_{50} = 4.6 ± 0.5 μM) among the C-2 chloro-PTZ derivatives.

The SAR studies of PTZs on BuChE inhibition indicates that, they were generally weak inhibitors compared to their inhibition profile toward AChE (Table 1). Among the non-chlorinated PTZs, compound **6a** exhibited superior inhibitory potency (BuChE IC_{50} = 5.8 ± 0.5 μM) relative to AChE (IC_{50} = 7.4 ± 0.6 μM) and was the most potent. It was approximately 11-fold more potent relative to the reference agent galantamine (BuChE IC_{50} = 66.5 ± 4.1 μM) and was less potent compared to both tacrine (BuChE IC_{50} = 0.04 ± 0.001 μM) and donepezil (BuChE IC_{50} = 3.6 ± 0.4 μM). Among the 2-Cl-PTZ derivatives **7g–l**, compound **7h** (R = benzyl), was identified as the most potent BuChE inhibitor (BuChE IC_{50} = 3.6 ± 0.4 μM). In general, the presence of a 2-Cl substituent led to enhanced BuChE inhibition potency for *N*-10 acyl PTZ derivatives **7g–j**. Interestingly, the presence of either a phenethyl (**7i**) or 4-methoxyphenyl (**7j**) *N*-10 acyl substituents, provided similar BuChE inhibition (IC_{50} values of 5.0 ± 0.6 and 5.3 ± 0.5 μM respectively) whereas both 3-methoxy (**7k**) and 3,4-dimethoxyphenyl (**7l**) derivatives exhibited weak inhibition (IC_{50} values of ~30.8 and 32.6 μM respectively). The cholinesterase SAR study for PTZ compound library demonstrates that they exhibit dual inhibition of both AChE and BuChE enzymes. They showed nonselective inhibition of both the cholinesterase enzymes and generally exhibited superior AChE inhibition potency.

The cholinesterase inhibition profile of PSZ derivative **12a** toward AChE, shows an IC_{50} value of 5.6 ± 0.4 μM and was less potent compared to reference agents tacrine (AChE IC_{50} = 0.16 ± 0.01 μM), donepezil (AChE IC_{50} = 0.04 ± 0.002 μM) and galantamine (AChE IC_{50} = 2.6 ± 0.6 μM, Table 2). However, it showed greater potency, than the organoselenium compound ebselen (AChE IC_{50} = 6.2 ± 0.5 μM). Addition of an *N*-10 phenyl substituent in compound **13a**, retained AChE inhibition (IC_{50} = 5.4 ± 0.4 μM) compared to **12a**. Compound **13b** (R = benzyl; AChE IC_{50} = 6.4 ± 0.6 μM) and **13c** (R = phenethyl; AChE IC_{50} = 6.7 ± 0.7 μM) were less potent

compared to **12a** (AChE IC_{50} = 5.6 ± 0.4 μM). The effect of methoxyphenyl substituents, at *N*-10 was explored by evaluating compounds **13d–f** (Table 2). Interestingly, these compounds exhibited AChE inhibition ranging from ~4.6 to 6.2 μM (IC_{50}). The 4-methoxyphenyl compound (**13d**) was identified as the most potent AChE inhibitor (IC_{50} = 4.6 ± 0.3 μM). Furthermore, the addition of a C-2 chlorine to the PSZ scaffold was investigated. Similar to the PTZ series, the C-2 chlorine substituent was not a major factor in AChE inhibition. The C-2 chloro-PSZ derivatives **12b** and **13g–l**, exhibited IC_{50} values in the range of ~5.8–6.5 μM (Table 2). Similar to the compounds from the non-chlorinated PSZ series (**12a** and **13a–c**), the presence of methoxyphenyl substituents, enhanced AChE inhibition (**13j–l**), with compound **13j** (R = 4-methoxyphenyl) identified as the most potent compound (AChE IC_{50} = 5.8 ± 0.4 μM), among the C-2 chloro-PSZ derivatives. The SAR studies of PSZs on BuChE inhibition indicates that, they were generally weak inhibitors compared to their inhibition profile toward AChE (Table 2). Among the non-chlorinated PSZs (**12a** and **13a–f**), compound **12a** exhibited superior inhibitory potency (BuChE IC_{50} = 3.0 ± 0.5 μM) relative to AChE (IC_{50} = 5.6 ± 0.4 μM) and was the most potent. It was approximately 22-fold more potent relative to the reference agent galantamine (BuChE IC_{50} = 66.5 ± 4.1 μM), and more potent than both donepezil (BuChE IC_{50} = 3.6 ± 0.04 μM) and ebselen (BuChE IC_{50} = 4.6 ± 0.6 μM). However, it was less potent compared to tacrine (BuChE IC_{50} = 0.04 ± 0.001 μM). Among the 2-Cl-PTZ derivatives **12b** and **13g–l**, compound **13g** (R = phenyl), was identified as the most potent BuChE inhibitor (BuChE IC_{50} = 3.8 ± 0.1 μM). In general, the presence of a 2-Cl substituent, led to enhanced BuChE inhibition potency for *N*-10 acyl PSZ derivatives **13g**, **13h**, **13j** and **13l**, relative to the corresponding non-chlorinated *N*-acyl PSZ derivatives (**13a–f**). Interestingly, the presence of either a 4-methoxyphenyl (**13j**), or and 3,4-dimethoxyphenyl (**13l**) *N*-10 acyl substituents, provided similar

BuChE inhibition (IC_{50} values of ~4.9 and 5.7 μM respectively), whereas both 3-methoxyphenyl (**13i**) and phenethyl (**13k**) derivatives, exhibited weak inhibition (IC_{50} values of ~40.0 and 19.3 μM respectively). The cholinesterase SAR study for PSZ compound library, demonstrates that they exhibit dual inhibition of both AChE and BuChE enzymes. Their AChE inhibition ranged from ~4.6-6.7 μM (IC_{50}s), whereas their BuChE inhibition ranged from ~3.0-40.0 μM. Similar to that of the PTZ series, the PSZ series exhibited nonselective inhibition of both cholinesterase enzymes, and generally exhibited superior AChE inhibition potency. These studies show that both PTZ and PSZ based compounds serve as useful ring scaffolds to design dual cholinesterase inhibitors.

2.3. Molecular docking studies of PTZ (**6a**, **7j**) and PSZ (**12a**, **13j**) compounds with human cholinesterases

The catalytic site of cholinesterases consists of His, Ser and Glu triad which are involved in substrate hydrolysis, whereas an anionic subsite consists of a Trp residue. In addition, the active site of AChE is made up of a peripheral anionic site (PAS) which is lined by amino acid residues Trp72, Asp74, Tyr124, Trp286 and Tyr341, whereas BuChE lacks this PAS due to the presence of smaller aliphatic amino acid residues closer to the entrance. As a consequence, BuChE active site is more than 60% larger (501.91 $Å^3$) compared to AChE (302.31 $Å^3$). The cholinesterase inhibitor tacrine is known to bind in the catalytic site and the anionic subsite.[22, 35]

Binding mode of **6a** (AChE IC_{50} = 7.4 ± 0.6 μM; BuChE IC_{50} = 5.8 ± 0.5 μM), within the active site of human AChE, shows that the tricyclic PTZ ring was oriented closer to catalytic and anionic subsites (His447 and Trp86 respectively). The aromatic rings of **6a**, underwent π-π stacking interactions with aromatic rings of Trp86, Tyr337 and Tyr341, whereas the central thiazine ring was in van der Waal's contact with Trp86 and Tyr337 (distance < 5 Å) as shown in

Figure 2a. Interestingly, the sulfur atom of thiazine ring was in van der Waal's contact with His447 (sulfur-π interaction, distance < 5 Å). Modeling of **6a** in the human BuChE shows that the PTZ ring was oriented in a flipped conformation compared to its binding mode in AChE (Figure 2b). The aromatic rings of **6a** underwent van der Waal's interactions with Trp82 and Ala328. These studies show that **6a** was able to inhibit cholinesterases through hydrophobic interactions.

The modeling study of the best PTZ derivative **7j** (AChE IC_{50} = 5.9 ± 0.6 μM; BuChE IC_{50} = 5.3 ± 0.5 μM, Figure 2c) shows that, in the AChE active site, the tricyclic PTZ ring, with a C-2 chloro substituent, underwent π-π and π-halogen interactions with Trp86, Tyr337 and Phe338 (Figure 2c). The central thiazine sulfur was closer to His447 (distance < 5 Å). The *N*-10 acyl amide C=O formed a hydrogen bond with hydroxyl of Tyr337 (distance = 2.7 Å) and the 4-methoxyphenyl substituent was in the vicinity of Asp74, Trp86, and Tyr124 (Figure 2c) closer to the PAS. Compound **7j** exhibits a different binding mode in BuChE, where the flipped PTZ ring undergoes π-π stacked and π-halogen interactions with Trp82 (Figure 2d). The sulfur atom of central thiazine ring was closer to Trp82 (distance < 5 Å). The 4-methoxyphenyl substituent underwent nonpolar contacts with Gly117 and Phe329.

The binding mode of selenium containing tricyclic **12a** (AChE IC_{50} = 5.6 ± 0.4 μM; BuChE IC_{50} = 3.0 ± 0.5 μM), in AChE active site, shows that the PSZ ring undergoes π-π interactions with Trp86, Tyr341 and Phe338 (distance < 5 Å, Figure 3a) and the selenium atom was in close proximity to Trp86. In the BuChE active site, **12a** exhibited a flipped conformation compared to its binding mode in AChE (Figure 3b), with the selenium atom closer to His438 (distance < 5.5 Å) and the tricyclic PSZ ring underwent a number of nonpolar contacts with Trp82, Ala328, Tyr338 and Tyr341 (distance < 5 Å). The binding mode of 4-methoxyphenyl compound **13j**

(AChE IC_{50} = 5.8 ± 0.4 μM; BuChE IC_{50} = 4.9 ± 0.5 μM, Figure 3c), in AChE, shows that the PSZ ring was closer to the anionic subsite and catalytic site, where it undergoes π-π and π-halogen interactions with Trp86 (distance < 5 Å). The selenium atom was closer to His447 and Tyr337 (distance < 4.5 Å). Interestingly, the *N*-10 acyl amide C=O formed a hydrogen bond with Tyr337 (distance = 2.7 Å) and the 4-methoxyphenyl moiety was oriented closer to the PAS (Tyr124), as shown in Figure 3c. In the BuChE active site, the PSZ ring of **13j**, was in van der Waal's contact with Trp82 and Ala328 (distance < 5 Å), whereas the 4-methoxyphenyl substituent was oriented toward the mouth of BuChE and underwent T-shaped π-π stacking interactions with Tyr332 (Figure 3d). These studies suggest that PTZ compound **7j** and PSZ compound **13j**, exhibit bivalent inhibition of AChE where the tricyclic ring was oriented closer to the catalytic and anionic subsite whereas the N-10 4-methoxyphenyl moiety was closer to the PAS.

2.4. Self-induced amyloid aggregation ($A\beta_{1-42}$) inhibition studies

The PTZ (**6a**, **6b**, **7f** and **7l**) and PSZ (**12a**, **12b**, **13f** and **13l**) compounds were evaluated for their ability to inhibit self-induced $A\beta_{1-42}$ aggregation, using the thioflavin-T (ThT) based fluorescence measurements (Table 3). Their activity was compared to a known Aβ-aggregation inhibitor, orange G (Table 3). The unsubstituted PTZ (**6a**), exhibited superior anti-aggregation activity compared to orange G at all concentrations tested (62% inhibition at 25 μM, Table 3), whereas **7f** was inactive. A similar trend was observed for C-2 chloro PTZ compounds **6b** and **7l** (60.8% and 5.9% inhibition at 25 μM, Table 3). Among the PSZ compounds tested, the *N*-10 unsubstituted PSZs, **12a** and **12b**, exhibited good anti-aggregation activity (45.6 and 45.0% inhibition respectively, at 25 μM Table 3), whereas *N*-10 acyl substituted compounds **13f** and **13l**, exhibited

weak anti-aggregation activity at the highest concentration tested (~11.0 and 5.9% inhibition respectively, at 25 μM, Table 3). The Aβ-aggregation kinetics data for compounds **6a** and **12a** is shown in Figure 4a and 4b. Both compounds were able to exhibit a concentration dependent decline in ThT fluorescence intensity over a period of time. The chart shows that both **6a** and **12a**, were able to produce a rapid decline in the Aβ-growth phase and reduce the formation of Aβ fibrils.

2.5. 2,2-Diphenyl-1-picrylhydrazyl (DPPH) radical scavenging activity

The antioxidant properties of PTZ (**6a**, **6b**, **7f** and **7l**) and PSZ (**12a**, **12b**, **13f** and **13l**) compounds, were evaluated using the DPPH radical scavenging activity and was compared with known radical scavenger trolox, and the organoselenium compound ebselen (Table 4).[36] The PTZ compound **6a**, (92.1% inhibition at 50 μM) exhibited excellent antioxidant activity. The *N*-10 acyl substituted PTZ compound **7f**, exhibited radical scavenging activity (44.3% inhibition at 50 μM). However, it showed a 2-fold decrease in antioxidant activity compared to **6a**. Similarly, the 2-chloro PTZ compound **6b** (76.4% inhibition at 50 μM), and **7l** (46.5% inhibition at 50 μM) exhibited similar trends, with the *N*-10 acyl substitution, proving to be detrimental to antioxidant activity. All the PSZ compounds tested (**12a**, **12b**, **13f** and **13l**), exhibited superior antioxidant activity (38.3–84.4% inhibition at 50 μM, Table 4), compared to the organoselenium reference compound ebselen (34.7% inhibition at 50 μM). In general, as observed with PTZ based compounds, *N*-10 acylation led to a decline in their antioxidant properties (**13f** = 39%; **13l** = 38.3% inhibition at 50 μM, Table 4). This study shows that, the presence of a free amine at *N*-10, of either PTZ or PSZ rings, provides excellent antioxidant properties, whereas *N*-10 acylation reduces their ability to scavenge DPPH radicals. It is suggested that, this could be due to the formation of a resonance stabilized radical in PTZ and PSZ's, that possess a free NH group,

while *N*-acylation might compromise this stability and exhibit less efficient DPPH radical scavenging activity (Figure 5).

2.6. Cell death assay studies of PTZ and PSZ compounds in SH-SY5Y neuroblastoma cells

The cell toxicity of PTZ (**6a**, **6b**, **7f** and **7l**) and PSZ (**12a**, **12b**, **13f** and **13l**) compounds, were carried out in SH-SY5Y neuroblastoma cells, using the 3-(4,5-dimethylthiazol-2-yl)-2,5-diphenyltetrazolium (MTT) bromide assay (Figure 6).[34] In these assays, PTZ compounds **6a**, **6b**, **7f** and **7l** exhibited moderate to good cell viability (63.3–71.6% viability at 50 μM). In contrast, PSZ compounds **12a**, **13f** and **13l,** exhibited good to excellent cell viability (76.0–100% viability at 50 μM) and were superior to the selenium-containing reference compound ebselen (53.9% viability at 50 μM). The C-2 chloro substituted PSZ compound **12b**, exhibited toxicity compared to other compounds tested (43.0% viability at 50 μM). These studies indicate that PTZ and PSZ templates are viable scaffolds to design small molecules with multi-targeting activity.

3. Conclusion

We have developed a novel class of fused tricyclic PTZ and PSZ based molecules as multi-targeting agents to treat AD. Among the PTZ and PSZ derivatives with *N*-10 acyl substitution, a 4-methoxyphenyl group provided good cholinesterase inhibition. However, *N*-10 acyl substitution was detrimental to anti-Aβ aggregation and antioxidant properties. In contrast, *N*-10 non-acylated derivatives (**6a**, **6b**, **12a** and **12b**), were able to (i) target and inhibit both AChE and BuChE enzymes; (ii) prevent Aβ-aggregation and (iii) scavenge DPPH radicals. It is anticipated that our work will provide design strategies to develop novel disease-modifying therapies for AD.

4. Experiments

4.1. Chemistry

All solvents, reagents and compounds **6a** (10*H*-phenothiazine) and **6b** (2-chloro-10*H*-phenothiazine) were purchased from various commercial vendors (Acros Organics, Sigma Aldrich, and Alfa Aesar, USA) with minimum purity of 95% and were used without further purification. Melting points were determined using a Fisher-Johns apparatus and are uncorrected. ^{1}H NMR and ^{13}C NMR spectra were performed on a Bruker Avance (300 and 75 MHz respectively) series spectrometer using $CDCl_3$ or DMSO-d_6 as the solvent. Coupling constants (*J*-values) were recorded in hertz (Hz) and the following abbreviations were used to represent multiplets of NMR signals: s = singlet, d = doublet, t = triplet, m = multiplet, br = broad. Carbon multiplicities (C, CH, CH_2, CH_3) were assigned by DEPT 90/135 experiments. High-resolution mass spectrometry (HRMS) analysis was done through positive ion electrospray ionization (ESI) using a Thermo Scientific Q-Exactive™ mass spectrometer, Department of Chemistry, University of Waterloo. The mass spectrometry data for PSZ and PSZ derivatives are reported based on the most stable selenium isotope (^{80}Se). Combustion analysis was carried out by Analest, Department of Chemistry, University of Toronto and were within ± 0.4% of theoretical values for C, H and N elements. Crude product purification was done using flash chromatography with Merck 230-400 mesh silica gel. Thin-layer chromatography (TLC) was performed on a Merck 60F254 silica gel plates (0.2 mm) using three different solvent systems (5:1 EtOAc:MeOH, DCM, 5:1 hexane:EtOAc) and spots were visualized at UV 254 nm. The purity of final compounds were confirmed (> 95%) by running Agilent HPLC (1200 Infinity series) using an analytical column (Agilent Zorbax Eclipse XDB-C8 column with 4.6 x 150 mm

dimensions and 5 μm particle size) with 50:50 ACN/water in 0.1% v/v TFA as eluent and a flow rate of 1.5 mL/min (detection at UV 254 nm).

4.2. General method for the preparation of PTZ derivatives (7a-l)

To a mixture of phenothiazine (**6a**) or 2-Cl phenothiazine (**6b**) (0.40 g, 2.01 mmol) in 7 mL of anhydrous toluene at room temperature, the desired acyl chloride (R = phenyl, benzyl, phenethyl, 3-methoxyphenyl, 4-methoxyphenyl or 3,4-dimethoxyphenyl) was added (1.5 eq). The reaction mixture was refluxed overnight at 110 °C and was monitored by TLC. Upon completion, the excess toluene was evaporated in vacuo. The crude product was purified via flash chromatography using DCM as the solvent. Final compound yields ranged from 70–95%. Analytical data for PTZ derivatives **7a**–**l** is given below.

4.2.1. 10*H*-Phenothiazin-10-yl-(phenyl)methanone (7a): White solid (80%). mp: 175–177°C. ^{1}H NMR (300 MHz, DMSO-d$_6$): δ 7.63–7.55 (m, 2*H*), 7.49–7.41 (m, 2*H*), 7.40– 7.32 (m, 1*H*), 7.31–7.19 (m, 8*H*).

4.2.2. 1-(10*H*-Phenothiazin-10-yl)-2-phenylethanone (7b): Yellow solid (94%). mp = 153–155 °C. ^{1}H NMR (300 MHz, DMSO-d$_6$): δ 7.54 (d, *J* = 7.7 Hz, 2*H*), 7.41–7.31 (m, 5*H*), 7.24–7.18 (m, 4*H*), 7.11–7.06 (m, 2*H*), 3.83 (s, 2*H*).

4.2.3. 1-(10*H*-Phenothiazin-10-yl)-3-phenylpropan-1-one (7c): Yellow solid (77%). mp = 98–100 °C. ^{1}H NMR (300 MHz, DMSO-d$_6$): δ 7.57 (d, *J* = 7.8 Hz, 2*H*), 7.52 (dd, *J* = 7.7 *Hz*, 1.3, 2*H*), 7.35 (td, *J* = 7.7, 1.5 Hz, 2*H*), 7.31–7.23 (m, 2*H*), 7.21–7.00 (m, 5*H*), 2.85–2.63 (br s, 4*H*).

4.2.4. (4-Methoxyphenyl)-10*H*-phenothiazin-10-yl-methanone (7d): White solid (71%). mp = 170–175 °C. ^{1}H NMR (300 MHz, DMSO-d_6): δ 7.58–7.50 (m, 2*H*), 7.46–7.39 (m, 2*H*), 7.25–7.18 (m, 6*H*), 6.78 (d, J = 8.9 Hz, 2*H*), 3.69 (s, 3*H*); HRMS (ESI) m/z calcd. for $C_{20}H_{16}NO_2S$ $[M + H]^+$ 334.0902, found 334.0895.

4.2.5. (3-Methoxyphenyl)-10*H*-phenothiazin-10-yl-methanone (7e): White solid (83%). mp = 155–157 °C. ^{1}H NMR (300 MHz, DMSO-d_6): δ 7.58–7.51 (m, 2*H*), 7.46–7.38 (m, 2*H*), 7.26–7.18 (m, 4*H*), 7.14 (t, J = 7.8 Hz, 1*H*), 6.88 (dd, J = 8.0, 2.2 Hz, 1*H*), 6.84–6.77 (m, 2*H*), 3.60 (s, 3*H*); HRMS (ESI) m/z calcd. for $C_{20}H_{16}NO_2S$ $[M + H]^+$ 334.0902. Found 334.0895.

4.2.6. (3,4-Dimethoxyphenyl)-10*H*-phenothiazin-10-yl-methanone (7f): White solid (70%). mp = 176–178 °C. ^{1}H NMR (300 MHz, DMSO-d_6): δ 7.58–7.51 (m, 2H), 7.46–7.39 (m, 2H), 7.26–7.19 (m, 4*H*), 6.91–6.86 (m, 1*H*), 6.84–6.76 (m, 2*H*), 3.69 (s, 3*H*), 3.50 (s, 3*H*); ^{13}C NMR (75 MHz, DMSO-d_6): δ 167.4, 150.5, 147.7, 139.4, 131.3, 127.7, 127.2, 126.8, 126.6, 121.2, 112.0, 110.7, 55.5, 55.1; HRMS (ESI) m/z calcd. for $C_{21}H_{18}NO_3S$ $[M + H]^+$ 364.1007, found 364.1003.

4.2.7. 2-Chloro-10*H*-phenothiazin-10-yl (phenyl)methanone (7g): Yellow solid (80%) mp: 157-160°C. ^{1}H NMR (300 MHz, DMSO-d_6): δ 7.64 (d, J = 7.2 Hz, 2*H*), 7.48 (d, J = 7.7 Hz, 2*H*), 7.38 (td, J = 7.6 Hz, 3, 2*H*), 7.31–7.23 (m, 2*H*), 7.18–7.13 (m, 2*H*), 6.97– 6.90 (m, 2*H*).

4.2.8. 1-(2-Chloro-10*H*-phenothiazin-10-yl)-2-phenylethanone (7h): Yellow solid (94%). mp = 90–92 °C. ^{1}H NMR (300 MHz, DMSO-d_6): δ 7.74 (s, 1*H*), 7.65 (d, J = 7.81, 1*H*), 7.52–7.45 (m, 2*H*), 7.44–7.22 (m, 3*H*), 7.21–7.12 (m, 3*H*), 6.98–6.90 (m, 2*H*), 3.82 (s, 2*H*); HRMS (ESI) m/z calcd. for $C_{20}H_{15}ClNOS$ ($[M + H]^+$ 352.0562, found 352.0558.

4.2.9. 1-(2-Chloro-10*H*-phenothiazin-10-yl)-3-phenylpropan-1-one (7i): Yellow oil (95%). ^{1}H NMR (300 MHz, DMSO-d_6): δ 7.67 (s, 1H), 7.61–7.49 (m, 3H), 7.41–7.33 (m, 2H), 7.31–7.25 (m, 1*H*), 7.22–7.14 (m, 2*H*), 7.11 (d, J = 7.0 Hz, 1*H*), 7.08–7.00 (m, 2*H*), 2.83–2.65 (br s, 4*H*); HRMS (ESI) m/z calcd. for $C_{21}H_{17}ClNOS$ $[M + H]^+$ 366.0719, found 366.0717.

4.2.10. 2-Chloro-10*H*-phenothiazin-10-yl-(4-methoxyphenyl)methanone (7j): Yellow solid (94%). mp = 153–155 °C. ^{1}H NMR (300 MHz, DMSO-d_6): δ 7.68 (s, 1H), 7.60–7.51 (m, 2*H*), 7.36–7.30 (m, 1*H*), 7.29–7.14 (m, 5*H*), 6.81 (d, J = 8.7 Hz, 2*H*), 3.70 (s, 3*H*); HRMS (ESI) m/z calcd. for $C_{20}H_{15}ClNO_2S$ $[M + H]^+$ 368.0512, found 368.0510.

4.2.11. 2-Chloro-10*H*-phenothiazin-10-yl-(3-methoxyphenyl)methanone (7k): White solid (92%). mp = 140–142 °C. ^{1}H NMR (300 MHz, DMSO-d_6): δ 7.64 (s, 1*H*), 7.56 (t, J = 8.6 Hz, 2*H*), 7.37–7.26 (m, 2*H*), 7.26–7.13 (m, 3*H*), 6.91 (d, J = 8.3 Hz, 1*H*), 6.86–6.77 (m, 2*H*), 3.62 (s, 3*H*); HRMS (ESI) m/z calcd. for $C_{20}H_{15}ClNO_2S$ $[M + H]^+$ 368.0512, found 368.0509.

4.2.12. 2-Chloro-10*H*-phenothiazin-10-yl-(3,4-dimethoxyphenyl)methanone (7l): Yellow solid (73%). mp = 155–158 °C. ^{1}H NMR (300 MHz, DMSO-d_6): δ 7.69 (s, 1*H*), 7.60–7.52 (m, 2*H*), 7.37–7.31 (m, 1*H*), 7.29–7.15 (m, 3*H*), 6.92–6.77 (m, 3*H*), 3.70 (s, 3*H*), 3.51 (s, 3*H*); HRMS (ESI) m/z calcd. for $C_{21}H_{17}ClNO_3S$ $[M + H]^+$ 398.0617, found 398.0613.

4.3. Synthesis of α-iodinated 2-cyclohex-2-enone (9)

To a mixture of cyclohex-2-enone **8** (1 mL, 10.33 mmol) in 50 mL of 1:1 THF:H_2O, iodine (1.5 eq), DMAP (1 eq) and potassium carbonate (1.2 eq) was added. The reaction mixture was allowed to stir at room temperature for 30 min. Upon completion, the reaction mixture was diluted with EtOAc. The organic layer was washed with saturated sodium thiosulfate and 10%

HCl. The organic layer was separated and evaporated in vacuo and the crude product was purified via flash chromatography using DCM as the solvent to afford **9**.

4.3.1. 2-Iodocyclohex-2-enone (9): Yellow solid (70%). mp = 49–50 °C. ^{1}H NMR (300 MHz, DMSO-d_6): δ 7.78 (t, J = 4.4 Hz, 1*H*), 2.63–2.51 (m, 2*H*), 2.43–2.34 (m, 2*H*), 1.93 (quin, J = 6.3 Hz, 2*H*).

4.4. General method for the preparation of diphenylamines (11a and 11b)

To a mixture of **10** (aniline or 3-chloroaniline, 4.8 mmol) in 10 mL EtOH, **9** (1.2 eq) and p-TsOH (0.2 eq) were added. The reaction mixture was refluxed overnight at 75 °C. Upon completion, the reaction mixture was diluted with EtOAc. The organic layer was washed with 20% sodium bicarbonate and saturated brine solution. The organic layer was separated and evaporated in vacuo. The crude product was purified via flash chromatography using DCM as the solvent. Final compound yield ranged between 40–50%. Analytical data for **11a** and **11b** is given below.

4.4.2. Diphenylamine (11a): Yellow solid (50%). mp = 50–52 °C ^{1}H NMR (300 MHz, DMSO-d_6): δ 8.08 (s, 1*H*), 7.18 (t, J = 8.1 Hz, 4*H*), 7.02 (d, J = 8.1 Hz, 4*H*), 6.77 (t, J = 7.2 Hz, 2*H*). ^{13}C NMR (75 MHz, DMSO-d_6): δ 143.4, 129.1, 119.6, 116.7.

4.4.3. 3-Chloro-*N*-phenylaniline (11b): Brown oil (40%). ^{1}H NMR (300 MHz, DMSO-d_6): δ 8.36 (s, 1*H*), 7.30–7.22 (m, 2*H*), 7.19 (t, J = 8.1 Hz, 1*H*), 7.07 (d, J = 8.1 Hz, 2*H*), 7.01–6.93 (m, 2*H*), 6.88 (t, J = 7.3 Hz, 1*H*), 6.78 (d, J = 8.1 Hz, 1*H*).

4.5. General method for the preparation of PSZ compounds 12a and 12b

To a mixture of selenium (1.00 g, 12.79 mmol) in 5 mL of sulfolane, the appropriate diphenylamine (**11a** or **11b**) (2 eq), selenium dioxide (1.20 eq), and iodine (0.1 eq) were added.

The reaction mixture was sealed in a pressure vial with a Teflon bushing and placed in an oil bath at 150 °C for 5 hours. Upon completion, the reaction mixture was cooled to room temperature and was filtered through Celite plug using dichloromethane (DCM). The solvent was evaporated in vacuo and recrystallized using EtOH and then subsequently purified twice or thrice by flash chromatography using 5:1 hexanes:EtOAc as the eluent. Final compound yield ranged from 20–25%. Analytical data for **12a** and **12b** are given below.

4.5.1. 10*H*-Phenoselenazine (12a): Yellow solid (20%). mp = 195–197 °C. ^{1}H NMR (300 MHz, DMSO-d_6): δ 8.56 (s, 1*H*), 7.10–6.95 (m, 4*H*), 6.78–6.68 (m, 4*H*); ^{13}C NMR (75 MHz, DMSO-d_6): δ 142.1, 128.8, 127.8, 122.1, 115.1, 111.5; HRMS (ESI) m/z calcd. for $C_{12}H_{10}N^{80}Se$ $[M + H]^+$ 246.9900, found 246.9895. Anal. calcd. for $C_{12}H_{10}NSe$ (246.16): C 58.55, H 3.69, N 5.69; found: C 58.61, H 3.73, N 5.64.

4.5.2. 2-Chloro-10*H*-phenoselenazine (12b): Purple solid (26%) mp = 199–200 °C. ^{1}H NMR (300 MHz, DMSO-d_6): δ 8.74 (s, 1*H*), 7.14–6.97 (m, 3*H*), 6.83–6.66 (m, 4*H*); HRMS (ESI) m/z calcd. for $C_{12}H_9ClN^{80}Se$ $[M + H]^+$ 281.9588, found 281.9500.

4.6. General method for the preparation of PSZ derivatives 13a–l

To a mixture of **12a** or **12b** (0.356 mmol) in 7 mL of anhydrous toluene, the desired acyl chloride (R = phenyl, benzyl, phenethyl, 3-methoxyphenyl, 4-methoxyphenyl or 3,4-dimethoxyphenyl) was added (1.5 eq). The reaction mixture was refluxed overnight at 110 °C. Upon completion, the excess toluene was evaporated in vacuo. The crude product was purified via flash chromatography using DCM as the solvent. Some compounds required two columns to purify (**13f** and **13l**). Final compound yields ranged from 20–80%. Analytical data for compounds **13a**–**l** are given below.

4.6.1. 10*H*-Phenoselenazin-10-yl-(phenyl)methanone (13a): Yellow solid (87%). mp = 157–159 °C. ^{1}H NMR (300 MHz, DMSO-d_6): δ 7.73–7.65 (m, 2*H*), 7.45–7.39 (m, 2*H*), 7.26–7.13 (m, 9*H*); HRMS (ESI) m/z calcd. for $C_{19}H_{14}NO^{80}Se$ $[M + H]^+$ 352.0240, found 352.0235. Anal. calcd. for $C_{19}H_{13}NOSe$ (350.27): C 65.15, H 3.74, N 4.00; found: C 65.55, H 3.92, N 4.01.

4.6.2. 1-(10*H*-Phenoselenazin-10-yl)-2-phenylethanone (13b): Yellow solid (91%). mp = 111–113 °C. ^{1}H NMR (300 MHz, DMSO-d_6): δ 7.66 (d, J = 7.6 Hz, 4*H*), 7.40 (t, J = 7.6 Hz, 2*H*), 7.30–7.22 (m, 2*H*), 7.21–7.13 (m, 3*H*), 6.99–6.90 (m, 2H), 3.72 (s, 2*H*); HRMS (ESI) m/z calcd. for $C_{20}H_{16}NO^{80}Se$ $[M + H]^+$ 366.0397, found 366.0393. Anal. calcd. for $C_{20}H_{15}NOSe$ •0.1 CH_2Cl_2 (372.79): C 64.76, H 4.11, N 3.76; found: C 64.96, H 3.76, N 3.82.

4.6.3. 1-(10*H*-Phenoselenazin-10-yl)-3-phenylpropan-1-one (13c): White solid (87%). mp = 184–186 °C. ^{1}H NMR (300 MHz, DMSO-d_6): δ 7.68 (d, J = 7.6 Hz, 2*H*), 7.57 (d, J = 7.8 Hz, 2*H*), 7.36 (t, J = 7.5 Hz, 2*H*), 7.28–7.06 (m, 5*H*), 7.02 (d, J = 7.2 Hz, 2*H*), 2.73 (s, 2*H*), 2.61 (br s, 2*H*); HRMS (ESI) m/z calcd. for $C_{21}H_{18}NO^{80}Se$ $[M + H]^+$ 380.0553, found 380.0546. Anal. calcd. for $C_{21}H_{17}NOSe$•0.1 H_2O (378.32): C 66.29, H 4.57, N 3.68; found: C 65.90, H 4.17, N 3.68.

4.6.4. (4-Methoxyphenyl)-10*H*-phenoselenazin-10-yl-methanone (13d): White solid (79%). mp = 184–186 °C. ^{1}H NMR (300 MHz, DMSO-d_6): δ 7.72–7.66 (m, 2*H*), 7.47–7.39 (d, J = 7.3 Hz, 2*H*), 7.27–7.13 (m, 6*H*), 6.76 (d, J = 8.7 Hz, 2*H*), 3.68 (s, 3*H*); HRMS (ESI) m/z calcd. for $C_{20}H_{16}NO_2{}^{80}Se$ $[M + H]^+$ 382.0346, found 382.0339. Anal. calcd. for $C_{20}H_{15}NO_2Se$•0.5 H_2O (389.30): C 61.70, H 4.14, N 3.60; found: C 61.82, H 4.09, N 3.57.

4.6.5. (3-Methoxyphenyl)-10*H*-phenoselenazin-10-yl-methanone (13e): White solid (84%). mp = 157–159 °C. ^{1}H NMR (300 MHz, DMSO-d_6): δ 7.71 (dd, J = 7.1, 1.7 Hz, 2*H*), 7.44

(d, *J* = 7.5 Hz, 2*H*), 7.29–7.09 (m, 5*H*), 6.92–6.77 (m, 3*H*), 3.60 (s, 3*H*); HRMS (ESI) m/z calcd. for $C_{20}H_{16}NO_2{}^{80}Se$ $[M + H]^+$ 382.0346, found 382.0338. Anal. calcd. for $C_{20}H_{15}NO_2Se \bullet 0.2\ H_2O$ (383.90): C 62.57, H 4.04, N 3.65; found: C 62.43, H 4.16, N 3.64.

4.6.6. (3,4-Dimethoxyphenyl)-10*H*-phenoselenazin-10-yl-methanone (13f): Yellow solid (73%). mp = 185–187 °C. ^{1}H NMR (300 MHz, DMSO-d_6): δ 7.71 (dd, *J* = 7.3, 1.7 Hz, 2*H*), 7.44 (dd, *J* = 7.7 Hz, 1.4, 2*H*), 7.14 (m, 4*H*), 6.93–6.87 (m, 1*H*), 6.84– 6.73 (m, 2*H*), 3.69 (s, 3*H*), 3.49 (s, 3*H*); ^{13}C NMR (75 MHz, DMSO-d_6): δ 167.3, 150.4, 147.6, 139.6, 130.3, 129.2, 127.8, 127.4, 126.8, 126.7, 122.1, 112.0, 110.7, 55.4, 55.2; HRMS (ESI) m/z calcd. for $C_{21}H_{18}NO_3{}^{80}Se$ $[M + H]^+$ 412.0451. Found 412.0445. Anal. calcd. for $C_{21}H_{17}NO_3Se \bullet 0.5\ H_2O$ (410.32): C 60.15, H 4.33, N 3.34; found: C 60.45, H 4.05, N 3.27.

4.6.7. 2-Chloro-10*H*-phenoselenazin-10-yl-(phenyl)methanone (13g): Yellow solid (79%). mp =155–158. ^{1}H NMR (300 MHz, DMSO-d_6): δ 7.78–7.68 (m, 3*H*), 7.37–7.13 (m, 9*H*); HRMS (ESI) m/z calcd. for $C_{19}H_{13}ClNO^{80}Se$ $[M + H]^+$ 385.9850, found 385.9841.

4.6.8. 1-(2-Chloro-10*H*-phenoselenazin-10-yl)-2-phenylethanone (13h): Yellow oil (73%). ^{1}H NMR (300 MHz, DMSO-d_6): δ 7.75 (br s, 1*H*), 7.67 (d, *J* = 8.3 Hz, 3*H*), 7.42 (t, *J* = 7.9 Hz, 2*H*), 7.37–7.23 (m, 2*H*), 7.23–7.12 (m, 2*H*), 6.95–6.88 (m, 2*H*), 3.74 (s, 2*H*); HRMS (ESI) m/z calcd. for $C_{20}H_{15}ClNO^{80}Se$ $[M + H]^+$ 400.0007, found 399.9998.

4.6.9. 1-(2-Chloro-10*H*-phenoselenazin-10-yl)-3-phenylpropan-1-one (13i): Yellow solid (84%). mp = 90–92 °C. ^{1}H NMR (300 MHz, DMSO-d_6): δ 7.74 (d, *J* = 8.5 Hz, 3*H*), 7.45–7.10 (m, 9*H*), 2.87–2.69 (br s, 4*H*); HRMS (ESI) m/z calcd. for $C_{21}H_{17}ClNO^{80}Se$ $[M + H]^+$ 414.0163, found 414.0155.

4.6.10. 2-Chloro-10*H*-phenoselenazin-10-yl-(4-methoxyphenyl)methanone (13j): White solid (47%). mp = 155–156 °C. ^{1}H NMR (300 MHz, DMSO-d$_6$): δ 7.78–7.64 (m, 3*H*), 7.31 (d, *J* = 8.2 Hz, 2*H*), 7.26–7.16 (m, 4*H*), 6.80 (d, *J* = 8.4 Hz, 2*H*), 3.70 (s, 3H); HRMS (ESI) m/z calcd. for $C_{20}H_{15}ClNO_2{}^{80}Se$ $[M + H]^+$); 415.9956, found 415.9947.

4.6.11. 2-Chloro-10*H*-phenoselenazin-10-yl-(3-methoxyphenyl)methanone (13k): Yellow solid (52%). mp = 135–137 °C. ^{1}H NMR (300 MHz, DMSO-d$_6$): δ 7.80–7.36 (m, 3*H*), 7.38–7.26 (m, 2*H*), 7.25–7.11 (m, 3*H*), 6.90 (d, *J* = 8.2 Hz, 1*H*), 6.86–6.78 (m, 2*H*), 3.61 (s, 3*H*); HRMS (ESI) m/z calcd. for $C_{20}H_{15}ClNO_2{}^{80}Se$ $[M + H]^+$ 415.9956, found 415.9947.

4.6.12. 2-Chloro-10*H*-phenothiazin-10-yl-(3,4-dimethoxyphenyl)methanone (13l): Yellow solid (28%). mp = 138–140 °C. ^{1}H NMR (300 MHz, DMSO-d$_6$): δ 7.78–7.65 (m, 3*H*), 7.35–7.26 (m, 2*H*), 7.24–7.15 (m, 2*H*), 6.96–6.73 (m, 3*H*), 3.69 (s, 3*H*), 3.50 (s, 3*H*); HRMS (ESI) m/z calcd. for $C_{21}H_{17}ClNO_3{}^{80}Se$ $[M + H]^+$ 446.0062, found 446.0054.

4.7. Cholinesterase inhibition studies

Human AChE and BuChE enzymes were obtained from Sigma-Aldrich, St. Louis, MO, USA (AChE product number C0663 and BuChE product number B4186 respectively). The inhibition profile of PTZ (**6a**, **6b** and **7a–l**) and PSZ (**12a**, **12b** and **13a–l**) series was evaluated using Ellman's reagent.[34] The cholinesterase inhibitors tacrine (item number 70240, Cayman Chemical Company, Ann Arbor, MI), donepezil (product number D6821, Sigma-Aldrich, St. Louis, MO) and galantamine (product number G1660, Sigma-Aldrich, St. Louis, MO) were used as reference agents. Test compounds were prepared as stock solutions in DMSO (maximum 1% v/v in final wells) and diluted in buffer solution (50 mM Tris.HCl, pH 8.0, 0.1 M NaCl, 0.02 M $MgCl_2.6H_2O$). Then in 96-well plates, 160 µL of 5,5'-dithiobis(2-nitrobenzoic acid) (1.5 mm

DTNB), 50 µL of *h*AChE (0.22 U/mL in 50 mm Tris.HCl, pH 8.0, 0.1% w/v bovine serum albumin, BSA) or 50 µL of *h*BuChE (0.12 U/mL in 50 mM Tris.HCl, pH 8.0, 0.1% w/v BSA) were incubated with 10 µL of test compounds (1, 5, 10, 25, 50 and 100 µM final concentrations) at room temperature for 5 min followed by the addition of 30 µL of either acetylthiocholine iodide (15 mM ATCl prepared in ultra pure water) or *S*-butyrylthiocholine iodide (15 mM BTCI prepared in ultra pure water). Then the absorbance was measured at various time intervals (0, 60, 120, 180, 240 and 300 s) at 412 nm. The inhibitory concentration (IC_{50} values) were calculated from the concentration–inhibition dose response curve on a logarithmic scale based on two independent experiments (n = 3).

4.8. Molecular modeling studies of PTZ and PSZ compounds in cholinesterases

Molecular docking experiments were performed using Discovery Studio (DS) Structure-Based-Design software program (version 4.0) from BIOVIA/Accelrys Inc. San Diego, USA. The coordinates for the X-ray crystal structures of human AChE was obtained from the protein data bank (pdb id – 4EY7). The protein was prepared using the *macromolecule* module in DS and active site was defined by selecting a 12 Å sphere around the ligand donepezil after which it was deleted. PTZ (**6a** and **7j**) and PSZ (**12a** and **13j**) compounds were built in 3D using the *small molecule* module in DS. The ligands were docked to AChE active site using CDOCKER algorithm using CHARMm force field. Docking steps include simulated annealing with 2000 heating steps, 700K heating target temperature and 5000 cooling steps, 300K cooling target temperature to generate 10 docked ligand poses. The enzyme-ligand complex obtained was ranked based on CDOCKER energy and CDOCKER interaction energy in kcal/mol. Polar and nonpolar contacts of ligands with cholinesterase enzymes were evaluated. A similar modeling

experiments were carried out to investigate the binding of ligands with human BuChE enzyme (pdb code = 2XQJ) after deleting the ligand VX 150.

4.9. Self-induced $A\beta_{1-42}$ aggregation inhibition studies

The anti-Aβ aggregation activity of test compounds (**6a**, **6b**, **7f**, **7l**, **12a**, **12b**, **13f** and **13l**), were evaluated using the ThT-based fluorescence assay. The $A\beta_{1-42}$ hexafluoro-2-propanol (HFIP) (rPeptide, Geogia, USA) stock solution was prepared by dissolving in 1% NH_4OH solution, to a 1mg/mL stock solution, followed by dilution in phosphate buffer (pH 8.0) to 500 μM. Stock solutions of test compounds were prepared in DMSO solution, diluted in phosphate buffer (pH 8.0), and were sonicated for 30 min. The final DMSO concentration per each well was 1% v/v or lower. The ThT fluorescent dye stock solution (15 μM) was prepared in 50 mM glycine buffer (pH 8.5). The aggregation kinetics assay was carried out using a Corning® 96-well flat, clear bottom black plates. Each well contains 110 μl of ThT, 50 μl of phosphate buffer (pH 8.0), 20 μl of test compounds in different concentrations (1, 5, 10 and 25 μM, final concentration) and 20 μl of $A\beta_{1-42}$ (5 μM final concentration). The plate was incubated at 37 °C with a plate cover under shaking and fluorescence was measured every 5 min. using a SpetraMax M5 multimode plate reader (excitation = 440 nm and emission = 490 nm) over a period of 16 h. Appropriate control experiments that contain $A\beta_{1-42}$ and test compound alone were evaluated as well. The known Aβ aggregation inhibitor orange G (Sigma-Aldrich, St. Louis, MO) was used as a reference compound. The percentage inhibition was calculated using the equation 100% control – [(IFi – IFo)] where 100% control indicates no inhibitor, IFi and IFo are the fluorescence intensities in the presence and absence of ThT. The results were expressed as percentage inhibition of two separate experiments of triplicate measurements.

5.0. Antioxidant activity evaluation

The DPPH radical scavenging activity of test compounds (**6a**, **6b**, **7f**, **7l**, **12a**, **12b**, **13f** and **13l**), were tested in a 96-well plate format. The antioxidants, trolox and ebselen were used as reference compounds. The test compound and DPPH (0.09 mM) stock solutions were prepared in methanol. The final test compound concentration was 50 μM. Each well contained 50 μL of test compound and 200 μL of DPPH solution. Appropriate controls with no DPPH and no test compounds were included. The 96-well plate was protected from light and incubated at room temperature with shaking for 60 minutes and then absorbance was measured at 517 nm. The percentage DPPH scavenging activity was calculated by subtracting the absorbance of the DPPH control by the difference in absorbance value of the test compounds and blank which was divided by the absorbance of the DPPH control. The value obtained was converted to percent inhibition. The results were expressed as mean ± standard deviation (SD) of two separate experiments (n = 3).

5.1. Cell death assay studies in SH-SY5Y neuroblastoma cells

The cell viability assay for test compounds (**6a**, **6b**, **7f**, **7l**, **12a**, **12b**, **13f** and **13l**) were carried out using SH-SY5Y neuroblastoma cells. They were plated at a density of 4 x10^5 per mL in 96-well plates with complete growth media consisting of DMEM and Ham's F12 in a 1:1 ratio, supplemented with 2.5 nM glutamate and 10% fetal bovine serum at 37 °C in 5% CO_2. The cells were incubated overnight and treated with the test compounds and ebselen (50 μM) for 24 h at 37 °C in triplicates (n = 3). The MTT reagent was added in 10% of the culture medium volume to each well and the cells were cultured for an additional 3 h at 37 °C in 5% CO_2. After incubation, the resulting formazan crystals were solubilized with MTT reagent solution in each well and the

absorbance was taken at 570 nm. All results were expressed as a relative percent of MTT to untreated controls.

Acknowledgements

The authors would like to thank Dr. John Honek, Department of Chemistry, University of Waterloo, for assistance with the fluorescence microplate reader, Ontario Mental Health Foundation for a PhD studentship (TM), NSERC-Discovery Grant to PR (RGPIN 03830-2014) and MB (RGPIN 371384-2013), Canada Foundation for Innovation (CFI-JELF) Leaders Fund (for PR) and Ministry of Research and Innovation, Government of Ontario, Canada for an Early Researcher Award (PR) for financial support.

Notes and references

1 R. Mayeux, Y. Stern, *Cold Spring Harb. Perspect. Med*., 2012, **2**, a006239.

2 C. Reitz, R. Mayeux, *Biochem. Pharmacol*., 2014, **88**, 640–651.

3 C. Reitz, C. Brayne, R. Mayeux, *Nat. Rev. Neurol*., 2011, **7**, 137–152.

4 J. S. Buckley, S. R. Salpeter, *Drugs Aging*, 2015, 32, 453–467.

5 J. Birks, *Cochrane Database Syst. Rev*., 2006, CD005593.

6 P. T. Francis, A. M. Palmer, M. Snape, G. K. Wilcock, *J. Neurol. Neurosurg. Psychiatry*, 1999, **66**, 137–147.

7 F. M. LaFeria, K. N. Green, S. Oddo, *Nat. Rev. Neurosci*., 2007, **8**, 499–509.

8 E. Karran, M. Mercken, B. D. Strooper, *Nat. Rev. Drug Discov*., 2011, **10**, 698–712.

9 L. M. Ittner, J. Gotz, *Nat. Rev. Neurosci*., 2011, **12**, 67–72.

10 E. Giacobini, G. Gold, *Nat. Rev. Neurosci*., 2013, **9**, 677–686.

11 M. P. Mazanetz, P. M. Fischer, *Nat. Rev. Drug Discov*., 2007, **6**, 464–479.

12 A. Gella, N. Durany, *Cell Adh. Migr*., 2009, **3**, 88–93.

13 M. Pohanka, *Curr. Med. Chem*., 2014, **21**, 356–364.

14 X. Wang, W. Wang, L. Li, G. Perry, H. G. Lee, X. Zhu, *Biochim. Biophys. Acta*. 2014, **1842**, 1240–1247.

15 A. Cavalli, M. L. Bolognesi, A. Minarini, M. Rosini, V. Tumiatti, M. Recanatini, C. Melchiorre, *J. Med. Chem*., 2008, **51**, 347–372.

16 M. Bajda, N. Guzior, M. Ignasik, B. Malawska, *Curr. Med. Chem*., 2011, **18**, 4949–4975.

17 W. J. Geldenhuys, C. J. Van der Schyf, *Expert Opin. Drug Discov*., 2013, **8**, 115–129.

18 M. I. Fernandez-Bachiller, C. Perez, G. C. Gonzalez-Munoz, S. Conde, M. G. Lopez, M. Villarroya, A. G. Garcia, M. I. Rodriguez-Franco, *J. Med. Chem*., 2010, **53**, 4927–4937.

19 Y. Wang, X. L. Guan, P. F. Wu, C. M. Wang, H. Cao, L. Li, X. J. Guo, F. Wang, N. Xie, F. C. Jiang, J. G. Chen, *J. Med. Chem*., 2012, **55**, 3588–3592.

20 M. T. Samara, H. Cao, B. Helfer, J. M. Davis, S. Leucht, *Eur. Neuropsychopharmacol.,* 2014, **24**, 1046–1055.

21 D. Taylor, Br. *J. Psychiatry Suppl*., 2009, **52**, S13–S19.

22 S. Darvesh, R. S. McDonald, A. Penwell, S. Conrad, K. V. Darvesh, , D. Mataija, G. Gomez, A. Caines, R. Walsh, E. Martin, *Bioorg. Med. Chem*., 2005, **13**, 211–222.

23 S. Darvesh, K. V. Darvesh, R. S. McDonald, D. Mataija, S. Mothana, O, Lockridge, E. Martin, *J. Med. Chem*., 2008, **51**, 4200–4212.

24 M. B. Borges, C. G. Dos Santos, C. H. Yokomizo, R. Sood, P. Vitovic, P. K. Kinnunen, T. Rodrigues, I. L. Nantes, *Free Rad. Res*., 2010, **44**, 1054–1063.

25 J. Lu, A. Holmgren, *J. Biol. Chem*., 2009, **284**, 723–727.

26 B. R. Cardoso, T. P. Ong, W. Jacob-Filho, O. Jaluul, M. I. Freitas, S. M. Cozzolino, *Br. J. Nutr*., 2010, **103**, 803–806.

27 Z. Luo, J. Sheng, Y. Sun, C. Lu, J. Yan, A. Liu, H. B. Luo, L. Huang, X. Li, *J. Med. Chem.,* 2013, **56**, 9089–9099.

28 Z. Wang, Y. Wang, W. Li, F. Mao, Y. Sun, L. Huang, Li X, *ACS Chem. Neurosci*., 2014, ***5***, 952–962.

29 D. Belei, C. Dumea, A. Samson, A. Farce, J. Dubois, E. Bicu, A. Ghinet, *Bioorg. Med. Chem Lett.,* 2012, ***22***, 4517–4522.

30 M. E. Kraft, J. W. Cran, *Syn. Lett*., 2005, ***8***, 1264–1266.

31 M. T. Barros, S. S. Dey, C. D. Maycock, *Eur. J. Org. Chem*., 2013, ***2013***, 742–747.

32 J. P. Duchesne, *US Pat.,* US5026846A, 1991.

33 J. Griffiths, S. A. Stephan, A. Bell, *US Pat*., US20070197494A1, 2007.

34 T. Mohamed, J. C. K. Yeung, M. S. Vasefi, M. A. Beazely, P. P. N. Rao, *Bioorg. Med. Chem. Lett.,* 2012, ***22***, 4707–4712.

35 L. Savini, A. Gaeta, C. Fattorusso, B. Catalanotti, G. Campiani, L. Chiasserini, C. Pellerano, E. Novellino, D. McKissic, A. Saxena, *J. Med. Chem*. 2003, ***46***, 1–4.

36 M. R. Szabo, C. Iditoiu, D. Chambre, A. X. Lupea, *Chem. Pap*., 2007, ***61***, 214–216.

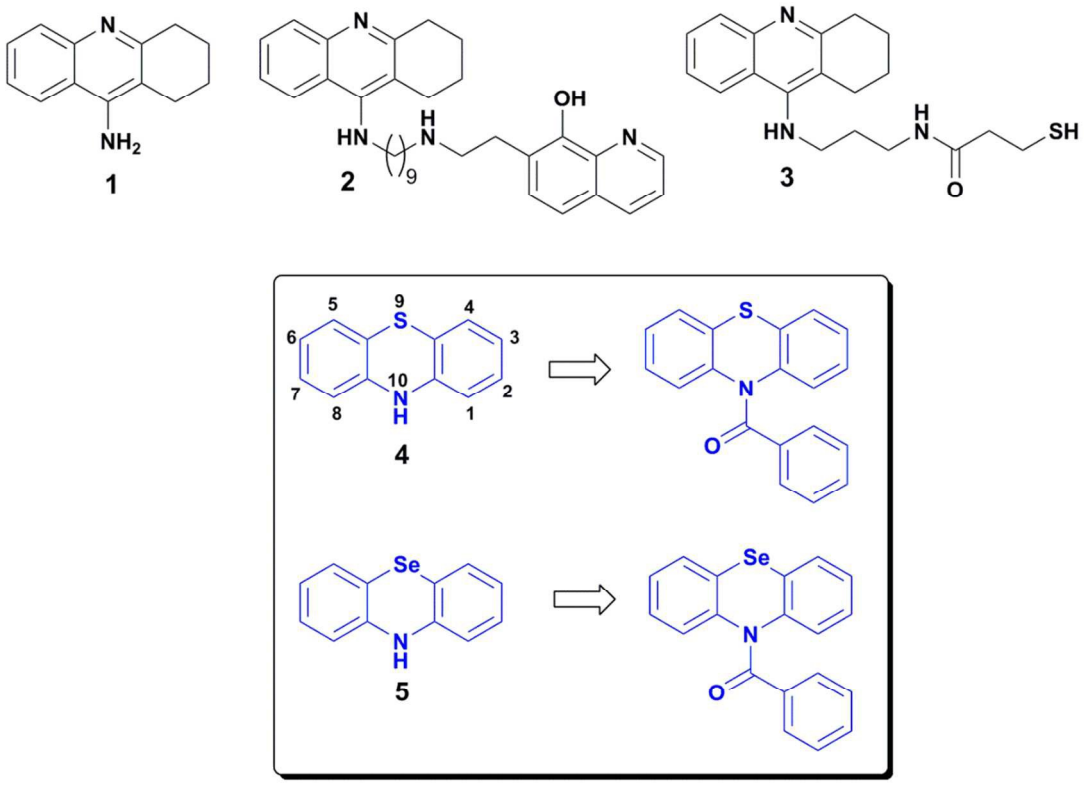

Fig. 1 Chemical structure of some fused tricyclic compounds **1**, **2**, **3**, **4** and **5**

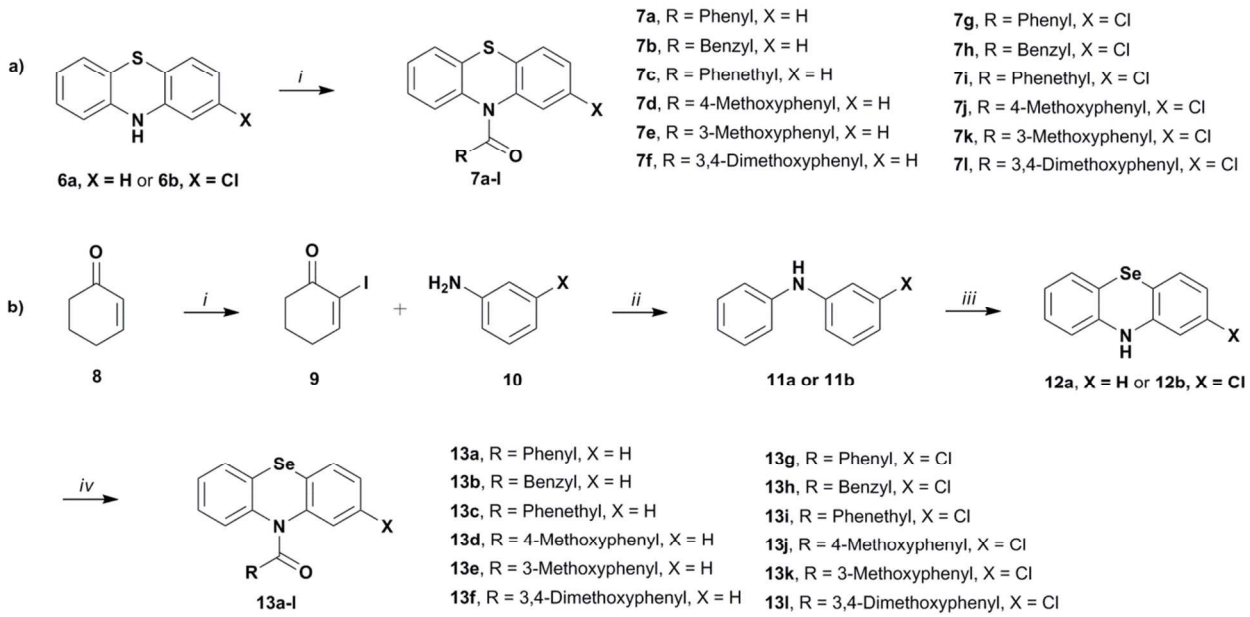

Scheme 1 a) Synthesis of compounds **7a–l**. Reaction conditions: (i) RCOCl (R = Phenyl, benzyl, phenethyl, 3- and 4-methoxyphenyl, and 3,4-dimethoxyphenyl), toluene, 110 °C reflux overnight; b) synthesis of compounds **12a**, **12b** and **13a–l**. Reaction conditions: (i) I_2, DMAP, K_2CO_3, THF:MeOH (1:1), r.t., 30 min; (ii) *p*-TsOH, ethanol, 75 °C reflux, 5 h; (iii) Se, SeO_2, I_2, sulfolane, 150 °C, pressure vial, 5 h; (iv) RCOCl (R = Phenyl, benzyl, phenethyl, 3- or 4- or 3,4-dimethoxyphenyl), toluene, 110 °C reflux overnight.

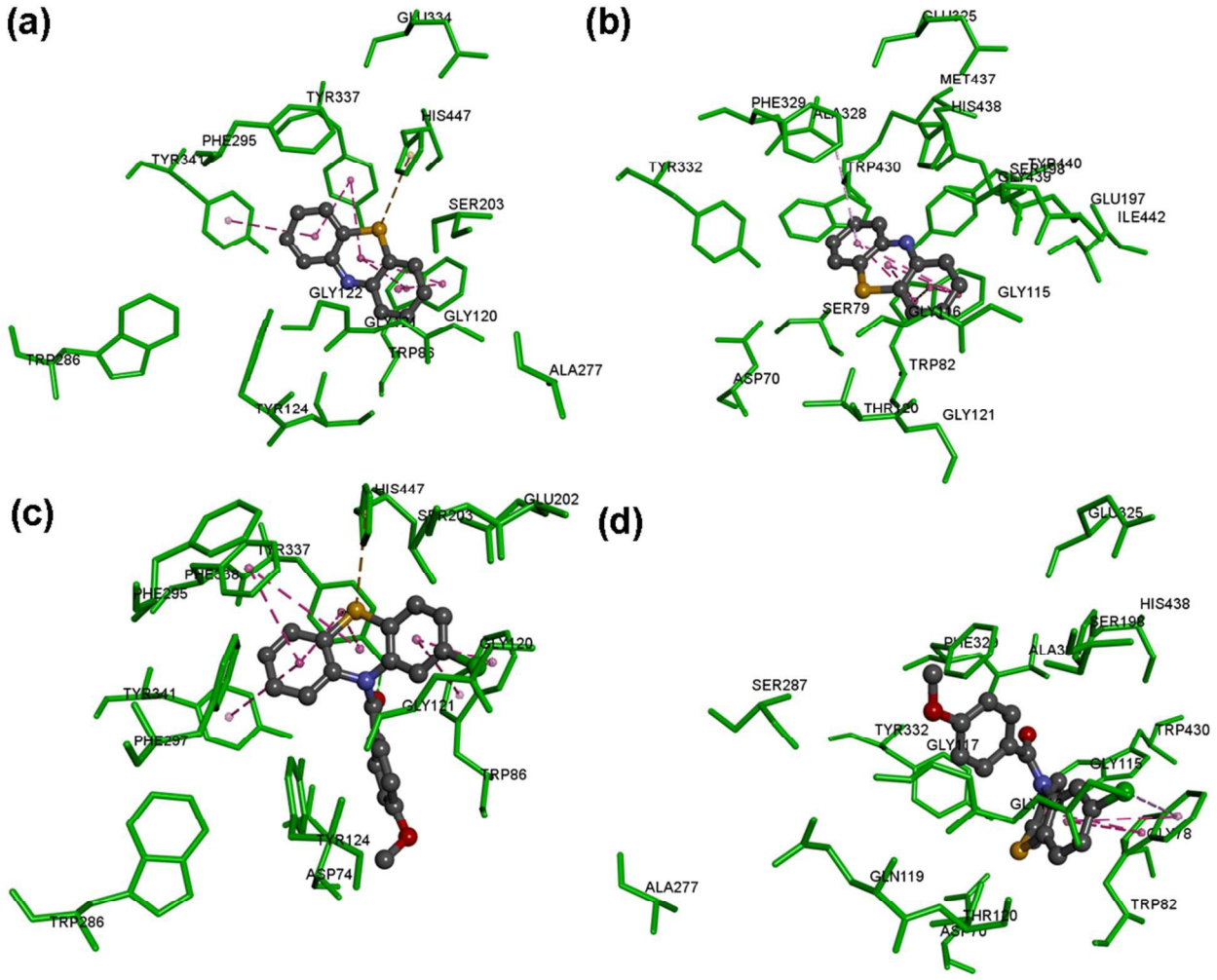

Fig. 2 Binding mode of PTZ compound **6a** (ball and stick cartoon) in the active sites of human AChE, CDOCKER interaction energy = –24.37 kcal/mol (a) and BuChE, CDOCKER interaction energy = –24.67 kcal/mol (b); Binding mode of PTZ compound **7j** (ball and stick cartoon) in the active sites of human AChE, CDOCKER interaction energy = –42.47 kcal/mol (c) and BuChE, CDOCKER interaction energy = –40.08 kcal/mol (d). Hydrogen atoms are removed for clarity.

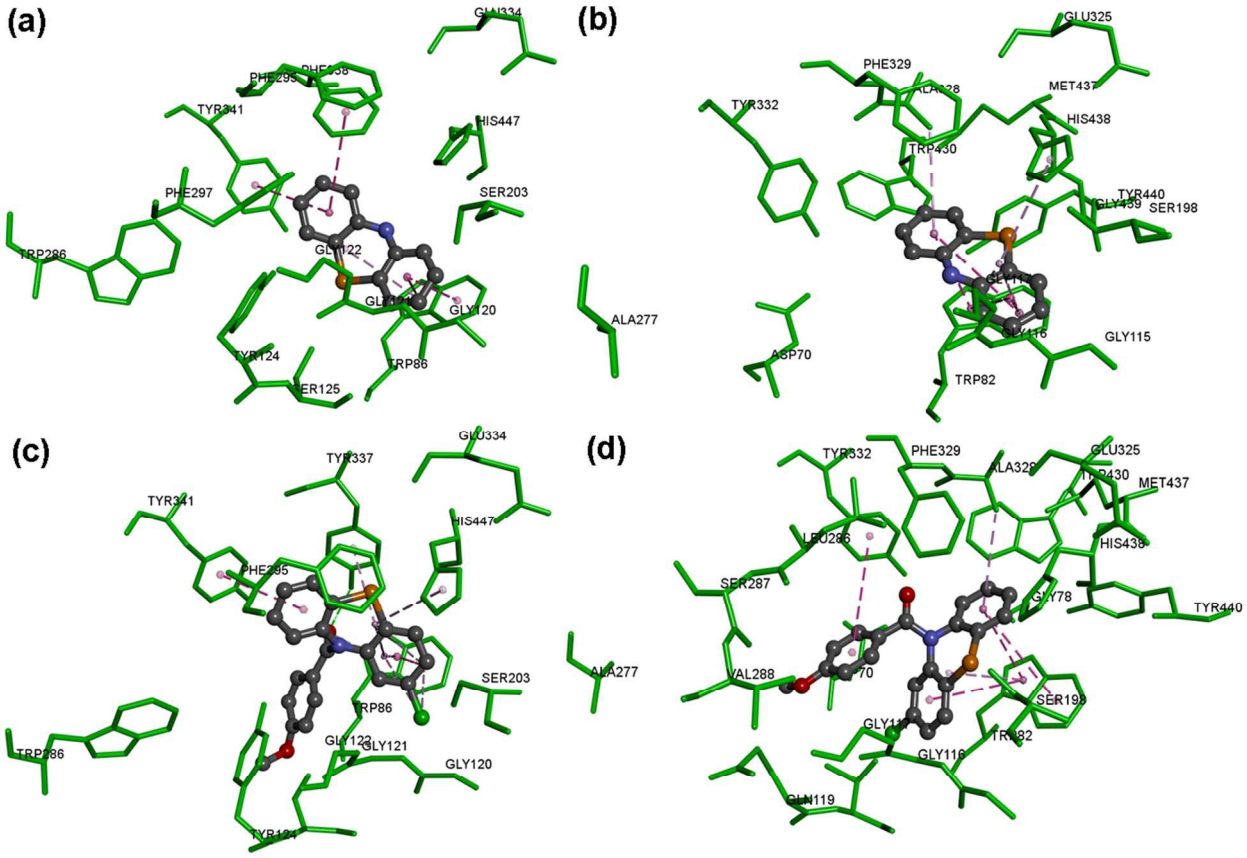

Fig. 3 Binding mode of PSZ compound **12a** (ball and stick cartoon) in the active sites of human AChE, CDOCKER interaction energy = –24.43 kcal/mol (a) and BuChE, CDOCKER interaction energy = –24.35 kcal/mol (b); Binding mode of PSZ compound **13j** (ball and stick cartoon) in the active sites of human AChE, CDOCKER interaction energy = –43.11 kcal/mol (c) and BuChE, CDOCKER interaction energy = –36.02 kcal/mol (d). Hydrogen atoms are removed for clarity.

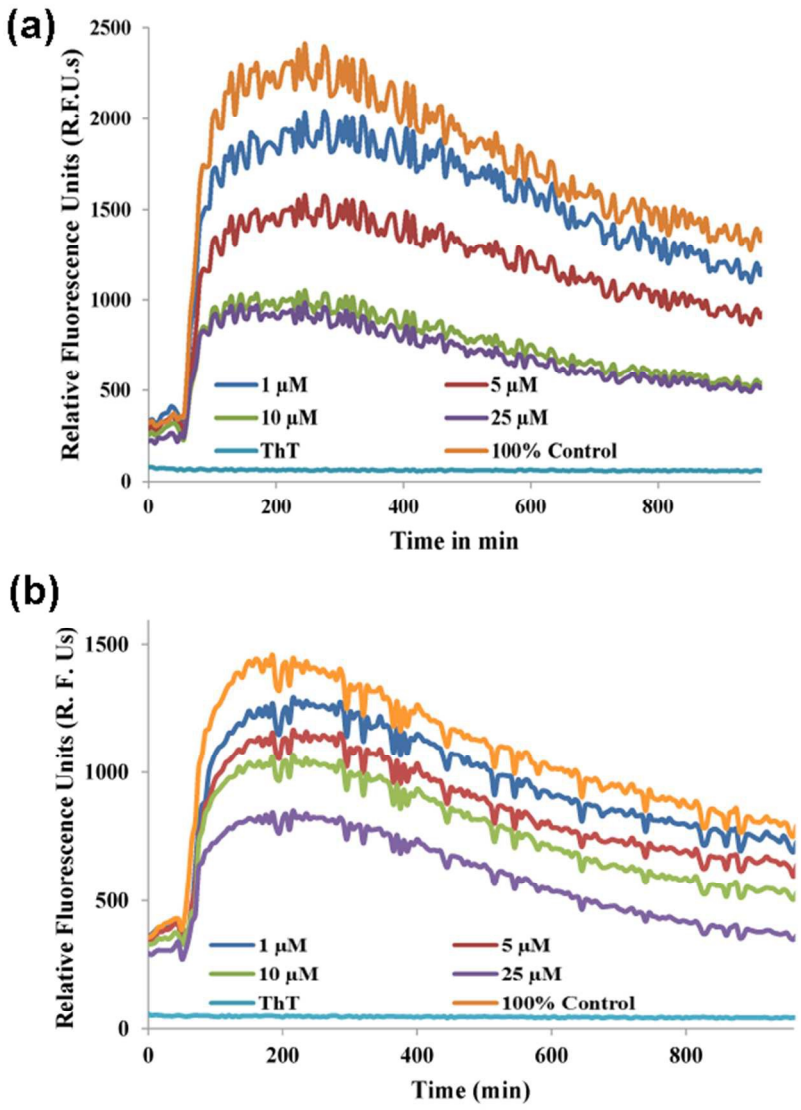

Fig. 4 (a) Time dependent, ThT based, self-induced, $A\beta_{1-42}$ aggregation kinetics assay profile at 37 °C (phosphate buffer pH 8.0) in the presence of PTZ compound **6a**; (b) Time dependent, ThT based, self-induced, $A\beta_{1-42}$ aggregation kinetics assay profile at 37 °C (phosphate buffer pH 8.0) in the presence of PSZ compound **12a**. 100% Control = Aβ only. Results are based on two independent experiments in triplicate measurements.

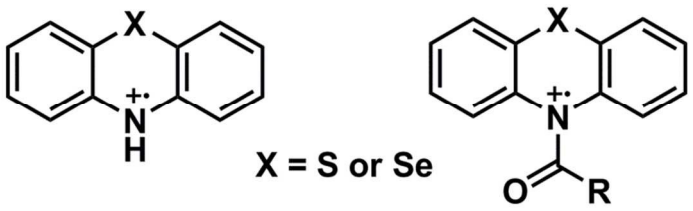

Fig. 5 Proposed antioxidant species of PTZ and PSZ based molecules

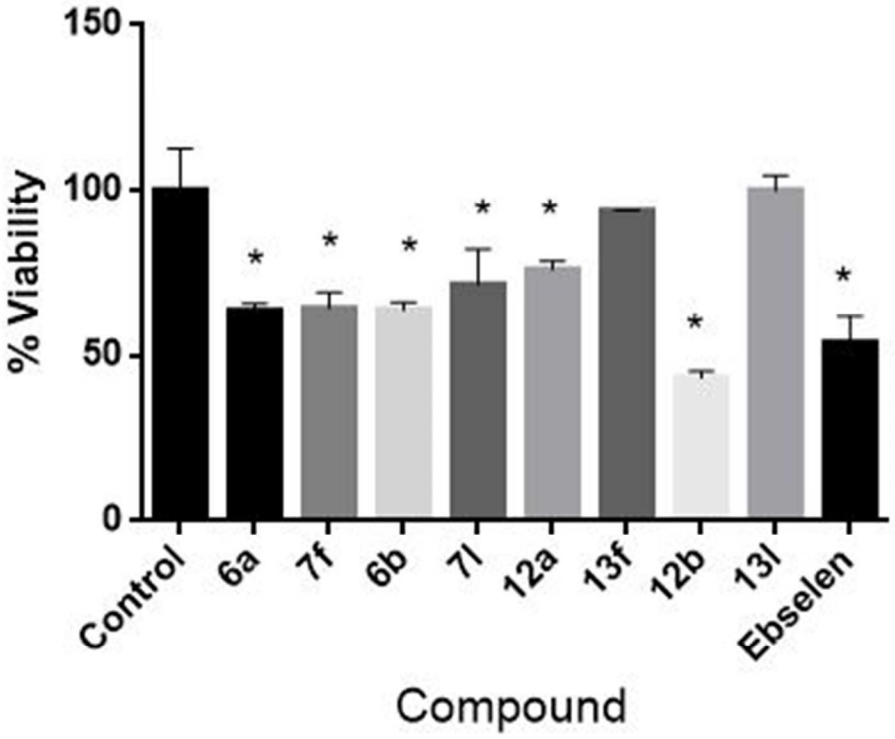

Fig. 6 Percent viability of SH-SY5Y neuroblastoma cell line after treatment with PTZ (**6a**, **6b**, **7f** and **7l**) and PSZ (**12a**, **12b**, **13f** and **13l**) compounds. [a]Percent inhibition values are average of two independent experiments (n = 3) with deviation <10% of mean value. * $p < 0.05$ compared to the control group (one-way ANOVA).

Table 1. Cholinesterase inhibition data, Selectivity Index and ClogP values of PTZ compounds **6a**, **6b** and **7a–l**

Compd	IC_{50} (μM)[a]		Selectivity	ClogP[c]
	AChE	BuChE	Index (SI)[b]	
6a	7.4 ± 0.6	5.8 ± 0.5	1.25	3.56
7a	8.0 ± 0.7	> 100	0.08	5.23
7b	7.4 ± 0.8	38.3 ± 2.7	0.19	3.87
7c	7.1 ± 0.8	51.0 ± 4.3	0.14	4.20
7d	6.3 ± 0.4	53.0 ± 4.9	0.11	5.45
7e	6.2 ± 0.6	25.5 ± 3.0	0.24	5.45
7f	5.8 ± 0.4	45.0 ± 5.0	0.12	4.59
6b	7.4 ± 0.9	19.2 ± 2.7	0.38	4.59
7g	9.9 ± 1.0	9.3 ± 0.8	1.06	6.00
7h	7.5 ± 0.6	3.6 ± 0.4	2.08	4.64
7i	7.9 ± 0.7	5.0 ± 0.6	1.58	4.97
7j	5.9 ± 0.6	5.3 ± 0.5	1.09	6.22
7k	4.6 ± 0.5	30.8 ± 2.0	0.14	6.22
7l	6.4 ± 0.7	32.6 ± 3.0	0.19	5.90
Tacrine	0.16 ± 0.01	0.04 ± 0.001	4.00	2.27
Donepezil	0.04 ± 0.002	3.6 ± 0.4	0.01	4.60
Galantamine	2.6 ± 0.6	66.5 ± 4.1	0.03	1.02

[a]IC_{50} values are average of two independent experiments (n = 3). [b]SI = *h*AChE/*h*BuChE IC_{50}. [c]ClogP was determined using ChemDraw Ultra version 11.0 Cambridge Software Company.

Table 2 Cholinesterase inhibition data, Selectivity Index and ClogP values of PSZ compounds **12a**, **12b** and **13a–l**

Compd	IC_{50} (μM)[a]		Selectivity	ClogP[c]
	AChE	BuChE	Index (SI)[b]	
12a	5.6 ± 0.4	3.0 ± 0.5	1.90	4.36
13a	5.4 ± 0.4	22.7 ± 0.1	0.24	6.03
13b	6.4 ± 0.6	11.0 ± 0.9	0.58	4.67
13c	6.7 ± 0.7	38.0 ± 4.0	0.18	5.00
13d	4.6 ± 0.3	11.1 ± 0.9	0.42	6.25
13e	6.2 ± 0.4	9.6 ± 0.8	0.65	6.25
13f	5.1 ± 0.4	9.1 ± 1.0	0.56	5.93
12b	6.3 ± 0.5	4.7 ± 0.6	1.33	5.37
13g	6.0 ± 0.7	3.8 ± 0.1	1.56	6.74
13h	6.5 ± 0.5	5.0 ± 0.3	1.31	5.38
13i	6.3 ± 0.6	40.0 ± 5.0	0.16	5.72
13j	5.8 ± 0.4	4.9 ± 0.5	1.18	6.96
13k	5.9 ± 0.7	19.3 ± 1.0	0.03	6.96
13l	6.2 ± 0.5	5.7 ± 0.6	1.07	6.64
Tacrine	0.16 ± 0.01	0.04 ± 0.001	4.00	2.27
Donepezil	0.04 ± 0.002	3.6 ± 0.04	0.01	4.60
Galantamine	2.6 ± 0.6	66.5 ± 4.1	0.04	1.02

Ebselen	6.2 ± 0.5	4.6 ± 0.6	1.34	3.70

[a]IC_{50} values are average of two independent experiments (n = 3). [b]SI = *h*AChE/*h*BuChE IC_{50}. [c]ClogP was determined using ChemDraw Ultra version 11.0 Cambridge Software Company.

Table 3: Self-induced amyloid ($A\beta_{1-42}$) inhibition data for PTZ (**6a**, **6b**, **7f** and **7l**) and PSZ (**12a**, **12b**, **13f** and **13l**) compounds

Compd	Percent Inhibition of Aggregation at [a]			
	1 μM	**5 μM**	**10 μM**	**25 μM**
6a	18.3 ± 2.0	37.2 ± 2.5	59.1 ± 4.3	62.0 ± 5.5
7f	NA	NA	NA	NA
6b	10.3 ± 1.2	22.0 ± 2.1	33.7 ± 3.2	60.8 ± 5.9
7l	6.2 ± 0.8	4.5 ± 0.5	6.5 ± 0.5	5.9 ± 0.6
12a	16.3 ± 1.5	24.1 ± 1.8	30.7 ± 3.1	45.6 ± 0.4
13f	6.3 ± 0.5	5.7 ± 0.6	8.7 ± 0.7	11.1 ± 0.8
12b	14.5 ± 1.3	18.5 ± 1.6	25.1 ± 1.9	45.0 ± 3.7
13l	8.4 ± 0.7	7.9 ± 0.9	9.1 ± 1.0	5.9 ± 0.6
Orange G	8.6 ± 0.8	20.4 ± 1.5	31.0 ± 2.5	57.2 ± 4.8

[a]Percent Aβ aggregation inhibition. Values are average percentage ± SD (n = 3) for two independent experiments. NA – Not active.

Table 4: DPPH radical scavenging activity of PTZ (**6a**, **6b**, **7f** and **7l**) and PSZ (**12a**, **12b**, **13f** and **13l**) compounds

Compound	**% DPPH scavenging at 50 µM**[a]
6a	92.1 ± 9.0
7f	44.3 ± 3.6
6b	76.4 ± 7.5
7l	46.5 ± 4.8
12a	84.4 ± 7.9
13f	39.0 ± 4.0
12b	73.2 ± 6.9
13l	38.3 ± 3.5
Ebselen	34.7 ± 3.2
Trolox	99.2 ± 8.7

[a]DPPH scavenging values are expressed as average percentage ± SD for two independent experiments (n = 3)